

FIRES: Fast Imaging and 3D Reconstruction of Archaeological Sherds

JIEPENG WANG, The University of Hong Kong
CONGYI ZHANG, The University of Hong Kong
PENG WANG, The University of Hong Kong
XIN LI, Texas A&M University
PETER J. COBB, The University of Hong Kong
CHRISTIAN THEOBALT, Max Planck Institute for Informatics
WENPING WANG, Texas A&M University

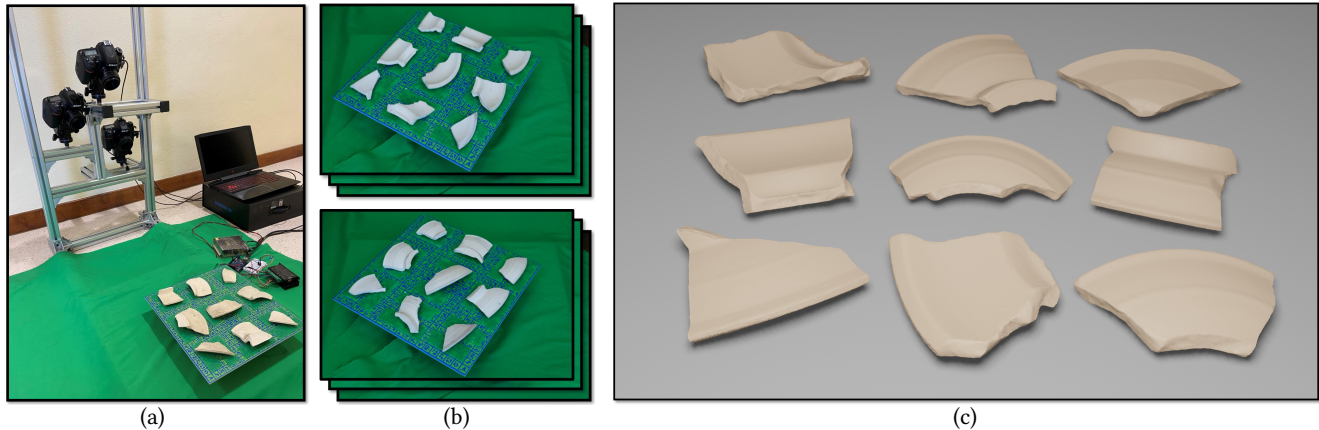


Fig. 1. Our proposed system, FIRES, has a high throughput of imaging over 700 sherds per day (8 working hours) with 3D reconstruction accuracy of $0.16mm$. (a) Fast image acquisition device, consisting of 3 cameras, a turntable and a PC controller; (b) Two reference images of the front sides and back sides of a batch of sherds; and (c) Reconstructed 3D sherds. With our reconstruction algorithm (Fig. 2), the 3D partial models of the front and back sides of a sherd are first reconstructed separately and then combined to produce the complete 3D sherd model.

Archaeology presents many research challenges for visual computing. An imperative task in archaeology is high-throughput imaging and 3D digital reconstruction of ceramic vessel fragments (or interchangeably, *sherds*). Sherds, as the most common artifacts uncovered during archaeological excavations, carry rich information about past human societies so need to be accurately reconstructed and recorded digitally for analysis and preservation. Often hundreds of fragments are uncovered in a day at an archaeological excavation site, far beyond the scanning capacity of existing imaging systems. Hence, there is high demand for a desirable image acquisition system capable of imaging hundreds of fragments per day. Such a system also needs to be portable, low-cost, and effective – the images acquired need to be of sufficient coverage and accuracy to allow precise 3D reconstruction of the fragments. In response to this demand, we developed a new system, dubbed *FIRES*, for Fast Imaging and 3D REconstruction of Sherds. The FIRES system consists of two main components. The first is an optimally designed fast image acquisition device capable of capturing over 700 sherds per day (in 8 working hours) in actual tests at an excavation site, which is one order-of-magnitude faster than existing systems, while meeting all the above requirements. The device consists of three commodity RGB cameras and a control system for capturing the images of sherds in a batch mode with minimal user assistance. The second component is a pipeline for 3D reconstruction of the sherds

from the images captured by the imaging acquisition system. It can accomplish the reconstruction of 700 sherds in about 10 hours on a commodity PC, achieving reconstruction accuracy of $0.16mm$. The pipeline includes a novel batch matching algorithm that matches partial 3D scans of the front and back sides of the sherds and a new ICP-type method that registers the front and back sides sharing very narrow overlapping regions. Extensive validation in labs and testing in excavation sites demonstrated that our *FIRES* system provides the first fast, accurate, portable, and cost-effective solution for the task of imaging and 3D reconstruction of sherds in archaeological excavations.

CCS Concepts: • Computing methodologies → Reconstruction; Matching.

Additional Key Words and Phrases: Digital Humanities, Archaeology, 3D Data Capture, Object Analysis, Photogrammetry, Efficiency

1 INTRODUCTION

1.1 Background

The human past is a finite resource. Throughout the world, ancient sites face threats of being destroyed from settlement development, conflict, looting, erosion, and climate changes. Archaeologists work carefully every day to record as many data as possible about the objects and architecture from past societies, but their precise scientific documentation efforts are time-consuming. In particular, during excavations archaeologists usually uncover tens of thousands of

Authors' addresses: Jiepeng Wang, The University of Hong Kong; Congyi Zhang, The University of Hong Kong; Peng Wang, The University of Hong Kong; Xin Li, Texas A&M University; Peter J. Cobb, The University of Hong Kong; Christian Theobalt, Max Planck Institute for Informatics; Wenping Wang, Texas A&M University.

ancient objects per month, but they face critical physical storage limitations [Di Angelo et al. 2018; Kersel 2015]. Digital data capture can help preserve a significant amount of crucial information about the human past [Roosevelt et al. 2015]. Over the last decade, most archaeologists have begun to capture 3D models of sites and objects - data that can be used both to study the past and to preserve information for the future. However, efficient digital capture remains as a challenge, which we took on through interdisciplinary collaboration between engineers and archaeologists [Cobb et al. 2019]. In this paper we address the problem of efficient recording of sherds (i.e., ceramic vessel fragments uncovered in archaeological excavations), also called *fragments* interchangeably.

The problem is enormous and imperative. For example, a typical excavation in the Middle East may easily uncover between 500 and 2000 sherds each day. Most excavations can only run during summer months due to weather and working calendar constraints. The primary focus of the excavator is to dig, thus leaving little time for documentation. Yet, many archaeologists have limited time to work on-site. Thus, they face the dual problems of not having enough time to work with the objects they uncover when they are with these materials at an excavation site, and of lacking direct access to the information content of the objects most of the year when they are away from the region of excavation. Hence, there is a high demand for an **efficient** 3D data capture system for archaeological objects that is capable of recording **at least a few hundreds to a thousand** pieces during the 8 work hours of each day, a throughput of roughly 2 sherds per minute.

In terms of **capturing accuracy**, currently, there is no general standard on how precise the reconstructed models of sherds should reach for their preservation in archival quality. Although [Sapirstein 2018, p. 34] proposed that a desirable system should reach a precision of about 0.1 millimeters in the final 3D reconstruction of sherds, most existing approaches/systems in literature were not able to provide quantitative evaluation. Finally, most archaeologists have limited budgets, so the solution should also be **cost-effective**.

In this work, we present the first solution to this problem by contributing a fast batch-based image acquisition scheme, together with an efficient 3D reconstruction pipeline. Our system is *high-throughput, accurate, cost-effective, easy-to-use by laymen, involving minimal user assistance, and deployable on excavation sites*. To overcome the issue of lacking quantitative accuracy evaluation and facilitate comparative studies in this field, we also publish a data benchmark and provide a comprehensive quantitative accuracy evaluation for large-scale fragment/sherd capturing and reconstruction.

1.2 State of the Art

There are a number of previous works on capturing images of 3D objects for the purpose of 3D reconstruction, including archaeological fragments. These include the photogrammetry approach [Porter et al. 2015], structured light scanning [Ahmed et al. 2014], and laser scanning [Magnani 2014] techniques, to name just a few. Two main issues that hinder the efficiency and throughput of most existing data acquisition systems are that: 1) they can only capture and process a single fragment in each phase of scanning. The acquisition of each fragment, hence, could take several minutes to finish, including

the time of manually flipping over the fragment so that both sides of it can be photographed or scanned; and 2) they require tedious manual operations to register the two scanned sides together to get complete models, especially for the step of removing extraneous parts of reconstructed models in each side (Refer to Sec. 2.1). Hence, it is critical to be able to capture images of multiple sherds simultaneously and reconstruct their complete models automatically for improving the processing throughput.

Related to archaeological fragment acquisition, two previous methods attempted to speed up acquisition by scanning multiple sherds simultaneously [Fan et al. 2016; Karasik and Smilansky 2008]. The method in [Karasik and Smilansky 2008] uses a frame to support six hanging clips each holding a sherd. This method is relatively fast (about 1 min for each sherd). However, it cannot produce complete 3D models because part of a sherd is always occluded by the clip holding it. In the second method [Fan et al. 2016], multiple sherds are placed flat on a table and are scanned with structured light. This method needs to compute a set of optimized camera viewpoints to ensure a complete coverage and to plan a travel path of the camera among the viewpoints, resulting in a slow scanning speed, typically taking about 10 mins to scan just one side of each sherd on average. We also acquire images of multiple sherds placed on a table in a batch mode but use a different imaging scheme to achieve much higher acquisition throughput.

1.3 System overview

Our imaging and reconstruction system consists of two main components: *a custom-built image acquisition device* and *an automatic 3D reconstruction pipeline*. The acquisition device efficiently captures the images of multiple fragments in a batch mode, and the reconstruction pipeline performs multi-view reconstruction and automatic front-and-back matching and registration to obtain the complete 3D models of fragments from the acquired images.

Image acquisition scheme. The image acquisition device consists of three consumer-grade cameras installed on an aluminum frame, taking pictures on multiple fragments placed flat on a controllable turntable (See Fig. 1 (a)). The only manual operation needed during the acquisition process is to place the fragments, and flip them to the other side after the pictures of one side are taken (See Fig. 1 (b)). For each side, the turntable turns a full circle with 16 stops for the 3 camera to take pictures from different perspectives. Therefore, 48 photos are taken in total for the front sides. Similarly, 48 photos of the back sides are taken.

Reconstruction pipeline. The adoption of the batch-mode of imaging in our setting presents some unique challenges in 3D reconstruction. Specifically, new techniques are needed to match the front sides of the fragments with their corresponding backsides; and then a reliable algorithm is needed to register the corresponding front and back side of each fragment to produce its complete 3D model. The reconstruction pipeline has the following three steps, as illustrated in Fig. 2.

- (1) **Reconstructing partial 3D scans for both sides.** After multiple images are obtained for a group of fragments, first their front sides and then the back sides, the reconstruction starts with applying image segmentation and Multi-view Stereo

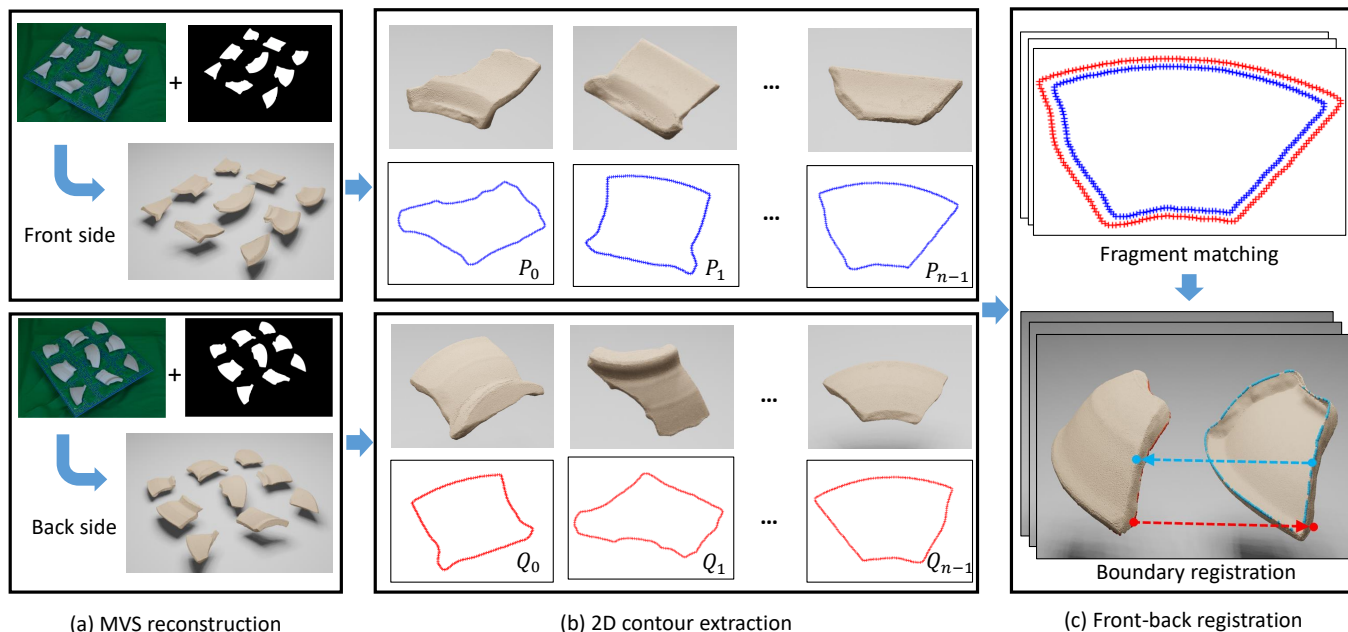


Fig. 2. **Overview.** (a) Given the images of two sides, we first perform multi-view reconstruction with selected image regions of two sides with high efficiency (Section 4). (b) With the reconstructed models, we then separate the models into individual fragments in each side and extract their maximum 2D contour (Section 4.1). (c) Based on these 2D contours, we propose a matching strategy to find correct matches of different fragments between their two sides. For each matching pair, local refinement is performed to get a complete and tight model (Section 4.2)

(MVS) to obtain the partial 3D models of the front and back sides of fragments in each batch, respectively.

- (2) **Matching partial scans from batches.** Next, to obtain each fragment’s complete 3D model automatically, we develop a new contour-based matching method to find the pairing of each fragment’s front side with its back side. This matching result also provides an initial alignment for the next registration step. Note that this front-back matching task is an outstanding research issue that has previously been encountered in a similar setting [Fan et al. 2016].
- (3) **Registering partial 3D scans.** Finally, after all the front-side scans are paired with their corresponding backsides, we register them to produce a complete 3D model using a novel, improved ICP model, called the *bilateral boundary ICP* (BBICP) method. This registration problem is particularly challenging because the front-side scans and back-side scans typically have small overlap. Existing ICP methods fail to achieve required robustness and accuracy due to such small overlap, as we will show later.

The details of these two components of our system will be presented in Section 3 and Section 4. Note that the design considerations of the two components are closely related. The imaging component is required to provide images with sufficient coverage and clarity to ensure that maximum reconstruction accuracy can be achieved in the 3D reconstruction phase. Meanwhile, the reconstruction pipeline must address difficulties arising from the particular batch mode employed during image acquisition.

1.4 Technical contributions

We made the following contributions in developing the first practical system, *FIRES*, for efficient imaging and reconstruction of sherds.

- **Efficient image acquisition:** We developed a fast image acquisition device that can capture and process images of multiple sherds simultaneously with minimal manual assistance (i.e. placing and flipping sherds on the scanning table). The device is capable of imaging over 700 sherds per day (in 8 working hours), which is a speedup of one order of magnitude over existing image acquisition systems and meets the throughput demanded by archaeological field work.
- **New methods for 3D reconstruction:** (1) To support the batch mode of image acquisition, we develop a matching algorithm to match the 3D front-side partial scans and the backsides from their batch acquisition, which is an outstanding problem in the literature; and (2) we develop an improved ICP method, called a *Bilateral Boundary ICP* (BBICP), for robustly and accurately registering the corresponding front and back sides of each fragment’s 3D partial scans to produce its complete 3D model.
- **A dataset for sherd acquisition and reconstruction:** To comprehensively validate the efficiency and accuracy of the proposed system, we built a dataset containing 123 fragments of different geometries, sizes, and textures. This dataset will be released to facilitate comparative studies in future research.

2 RELATED WORK

2.1 Image acquisition of sherds

Current data acquisition techniques can be generally categorized into 1) photogrammetry [Porter et al. 2015; Sapirstein 2018], 2) structured light scanning [Ahmed et al. 2014; Karasik and Smilansky 2008], and 3) laser scanning [Magnani 2014] based systems. Because of their cost, portability, and ease of usage, photogrammetry devices are more widely adopted in archaeology [Di Angelo et al. 2018]. In order to get a complete reconstruction, each object needs to be captured through multiple views. For example, the piece is often held to stand with the help of putty or an eraser. This setting, however, introduces tremendous manual labor and time during data acquisition. In the data processing stage, the merge of different sides of the objects also needs a laborious trimming to remove extraneous material. Users face the problems of frequent interactions and computer-processing time during the capturing and post-processing period to get complete models. Therefore, these existing approaches cannot scale beyond a few dozen objects per day.

To realize a larger scale data acquisition, [Karasik and Smilansky 2008] use a specially designed frame to hold multiple fragments for faster scanning. But this system fails to get complete models because part of the fragments are occluded by the frame. [Fan et al. 2016] propose a 3D scanning system that can digitize fresco fragments by scanning then merging the the two sides of multiple pieces. However, the view planning process is time-consuming, making the acquisition less efficient. Another unsolved problem of this system, as the authors stated, is how to automatically find matches between the two partial 3D scans of the front side and back side of each fragment for registering them to get a complete reconstruction.

There are also hardware systems that combine multiple types of devices to provide hybrid solutions to record different aspects of a target object. However, to our best knowledge, all existing systems [Hodan et al. 2017; Kaskman et al. 2019; Kasper et al. 2012; Singh et al. 2014] in this category focus on reconstructing only visible region of objects on the turntable rather than getting complete 3D models. Also, most of them do not consider efficiency to be a key requirement, and hence, involve tremendous labor during acquisition or post processing. So far, efficient large-scale data acquisition of pottery fragments remains an outstanding and challenging issue. We tackle this challenge by developing an image acquisition scheme that scans the front sides and then back sides of multiple sherds laid flat on a turntable.

2.2 Registration for 3D reconstruction

Since the image acquisition system captures the front sides and back sides of a group of fragments separately, an out-of-box MVS algorithm (i.e. OpenMVS [Cernea 2020]) is used to produce the partial 3D models for the front side and back side of each fragment separately. Hence, a 3D model registration method is needed for merging the front and back partial 3D scans to produce the complete 3D model of each fragment. A challenging issue here is that the these two partial scans only share a small overlap region, i.e. along the fractured strip surface. This poses a significant challenge to existing methods for reliable geometric registration.

Geometric registration [Tam et al. 2012] can be generally categorized into two types: global registration that finds a rough transformation between two surfaces, and local refinement that computes a precise transformation. Global registration methods are usually based on matches of local feature descriptors [Rusu et al. 2009; Zhou et al. 2016], tuples of points [Aiger et al. 2008; Mellado et al. 2014], or the branch-and-bound framework [Yang et al. 2015], while local refinement algorithms are often based on the iterative closest point (ICP) algorithm and its variants [Chetverikov et al. 2002; Pomerleau et al. 2013; Ying et al. 2009]. Branch-and-bound based methods are often very expensive and prohibitive in handling very dense point sets. Feature-based methods rely on salient texture or geometry features to find correct correspondence and transformations, which, unfortunately, are often unavailable on fragmented pieces. Tuples of points based methods and local refinement algorithms are sensitive to how much the two surfaces overlap with each other. However, between the front and back sides of each fragment, such an overlap is generally quite small.

ICP is also used in [Brown et al. 2008] to align the front side to the back side of fresco fragments by assuming all the pieces are flat. This strategy is not suitable for sherds because sherd surfaces have curved shapes that are more complex than frescoes. Hence, it is hard to directly apply the existing ICP methods to robustly registering the two partial scans of a sherd in our setting.

In this work we present two novel methods for 3D reconstruction – one for matching the front sides and back sides of the fragments to provide a good initialization for registration, and another for robust fine registration of the front and back partial 3D scans to form a complete 3D sherd mode in the presence of small overlap.

3 IMAGE ACQUISITION SCHEME

Our image acquisition scheme consists of a customized hardware system (see Fig. 1 (a)) and a batch capturing strategy. It is designed to meet the following requirements for high-throughput sherd capturing and reconstruction: (1) efficient acquisition; (2) sufficient coverage for accurate reconstruction; (3) minimal manual labor; (4) low cost; and (5) portable and easy to deploy in the field.

The hardware of the system has three main parts:

- A turntable consisting of a stepper motor, a stepper motor driver, an Arduino board [Badamasi 2014], and a flat board in printed ArUco patterns [Garrido-Jurado et al. 2014] for camera calibration;
- Three cameras mounted on an aluminum frame. They are at different heights to provide sufficient coverage of the vertical viewing range.
- A controller module running on a PC that controls the motion of the turntable and synchronizes the motion with the cameras shutters.

Acquisition procedure. To capture a *group* of fragments in a batch mode, we place them flat on the turntable, and first take a set of pictures to capture their exposed sides, to be called the *front sides*. Then the fragments are flipped manually on the turntable to photograph their *back sides*. We call all these pictures a *batch*. Three cameras are used to take the pictures and the turntable makes 16

stops to complete a full circle of rotation, i.e. with a rotation angle of 22.5° for each move. Therefore, each batch has $3 \times 16 = 48$ images.

The capturing of each batch of 48 images is controlled and synchronized by a PC controller. Once captured, the batch of images are transmitted to a PC for 3D reconstruction.

Efficiency and cost. We have tested this setup by placing 4 ~ 18 fragments on the turntable based on the size of fragments. Taking the 9-piece experiment as an example, the system captures both sides in less than 5 minutes, including the time to manually place and flip the fragments. The average time of capturing both sides of one sherd is about 0.5 minutes. The whole system is portable and can easily be assembled. The hardware costs about \$2,500 in total.

Design justification. In arriving at this setup of devices, we have tested different configurations with different numbers of cameras and images to take in a full circle. Our tests showed that the setup with three cameras provides better coverage in terms of vertical view angles for faithful 3D model reconstruction than those with one or two cameras; and using more cameras would unnecessarily increase the cost and complexity of the capturing device without noticeable improvement of reconstruction accuracy. Meanwhile, we found that taking 16 images by each camera in a full circle provides better coverage of the side view for accurate coverage than using substantially fewer images, while increasing the number of images to more than 16 will unnecessarily increase the time of image processing and without bringing noticeable accuracy improvement. Details of these experiments can be found in the supplementary.

Scale consistency. Image-based reconstruction often has an issue of scale ambiguity. Without a reference metric, 3D structures reconstructed from images taken in different passes may differ by a global scaling factor. To resolve this ambiguity, we used the ArUco codes on the patterned board, which have known sizes, to normalize the scale of the reconstructed models in world coordinates. More details of this scale calibration procedure can be found in the supplementary document.

Sliding prevention. When the turntable rotates with jerky “start stop” motions with large acceleration, the fragments may slide on the table due to lack of friction, causing errors in 3D reconstruction by MVS. To address this issue, we set the angular acceleration of the turntable to be 7 deg/s^2 , small enough to prevent the fragments from sliding. Meanwhile, the maximum angular speed is 12 deg/s , also small enough not to cause centrifugal movement of the fragments.

4 RECONSTRUCTION PIPELINE

Our reconstruction pipeline has three steps:

1. Reconstruct partial 3D models from images;
2. Match front- and back-sides of fragments from scan batches;
3. Register the two sides of a sherd into a complete 3D model.

In Step 1, given a set of images (e.g., the front side of fragments captured as a group), the goal is to reconstruct partial 3D models of these fragment. We first segment the sherd regions in these images and generate their masks using UNet [Ronneberger et al. 2015]. From these segmented regions, the partial 3D models (front side) of all the fragments on the table are then reconstructed using openMVS [Cernea 2020]. These result in multiple disjoint point clouds, each corresponding to one fragment (see some examples in Fig. 2 (a)).

Next, after these fragments are flipped, their back sides are processed similarly to produce partial 3D models (Fig. 2 (b)).

Since this Step 1 is a direct application of an existing MVS method, it reliably produces partial models. The challenges are in Steps 2 and 3, which require substantial modification/improvement from existing 3D reconstruction technologies. We elaborate these two steps in the following Sections 4.1 and 4.2.

4.1 Matching Front and Back Sides

With the reconstructed 3D partial models (i.e., the front and back sides) of the captured batches of fragments, before being able to registering the two sides together, we need to solve a pairing problem that connects each fragment’s front side with its respective back side. We call this problem of finding corresponding matches from two batches of 3D partial models a *front-back matching problem*. Note that this problem was encountered in [Fan et al. 2016] (which also attempts to scan fragments of fresco in groups) but was posed as an unsolved problem.

A naive but immediate solution to circumvent this matching problem is to ensure all the fragments remain in the (almost) same positions when being flipped over, and match the partial scans using their locations. However, during field tests, it was found that this strategy is error-prone, because operators sometimes would tend to adjust the positions of the pieces after flipping in order to better place and separate them, especially when there are many fragments in a group. This would then cause mismatches and result in failed reconstruction.

We present a shape matching scheme by developing 2D shape descriptors for partial models. This matching scheme is automatic and reliable. And it also provides an initial alignment (between the front and back sides) for the subsequent registration task.

Our observation is that most sherds, although curved in general, are relatively flat and can be approximately fitted by planes (e.g., through PCA). With this assumption, the 3D contour of a fragment can be approximated by the contour of its 2D projection on its fitting plane. We can then use a shape descriptor to encode each 2D contour, and then compare shape descriptors of these 2D contours to identify the pairing between each front side and its corresponding back side.

Shape descriptors of 2D contours.

Let C denote a 2D contour, represented by a closed simple polygon with a sequence of n_c vertices $\{v_i\}_{i=0}^{n_c-1}$ which are ordered clockwise with respect to the contour and equally spaced along the contour. Using *turtle graphics* [Sederberg et al. 1993], we represent the polygon by the sequence of turning angles $\{\theta\}_{i=0}^{n_c-1}$

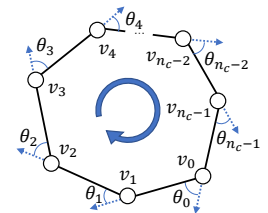


Fig. 3. Contour description.

at its vertices, where the turning angle is defined to be the angle between the two edges incident to a vertex of the polygon, as shown in Fig. 3. Note that the sequence of edge lengths in turtle graphics is unnecessary here because the vertices are equally spaced so all the edge lengths are equal, denoted by a constant ℓ . Evidently, the shape and size of the 2D shape C is completely encoded by the sequence

$\{\theta\}_{i=0}^{n_c-1}$ plus the common edge length ℓ . Then we define a sequence of the accumulative sums of the turning angles, $\{\Theta_i\}_{i=0}^{n_c-1}$, where $\Theta_i = \sum_{j=0}^i \theta_j$. The vector $\Theta = (\Theta_i)^T \in \mathbb{R}^{n_c}$ is called the *shape descriptor* of the 2D contour C . Here we use the accumulative sums of the turning angles as a shape descriptor, rather than the turning angles themselves, because the former is more robust to noise and small shape perturbation than the latter.

Since the shape descriptor $\Theta = (\Theta_i)^T$ depends on the choice of the starting vertex v_0 of the contour C , C has n_c equivalent shape descriptors, each determined by the starting vertex v_0 chosen. Hence a shape descriptor is denoted as $\Theta(C, v_0)$, to emphasize this dependence.

Computing contour shape descriptors. For the front 3D partial scan of a pottery fragment represented as a point cloud $\mathcal{P} = \{\mathbf{p}_i\}$, we first scale it to fit in a unit cube, then derive its projection onto its fitting plane obtained via PCA analysis [Wold et al. 1987], i.e. the plane passing through the centroid of the point cloud \mathcal{P} and with its normal vector being the eigenvector associated with the smallest eigenvalue of the co-variance matrix of \mathcal{P} . We then use Alpha Shape [Bernardini and Bajaj 1997] to extract the 2D contour of the projected 2D point cloud, and uniformly sample n_c points (we set $n_c = 200$) along the contour for computing the descriptor of the contour. Note that, the 2D contour of the *back* 3D partial scan of a pottery fragment is obtained in the same way, except that their derived 2D contour needs to be flipped before computing its shape descriptor because the shape descriptor is defined for boundary vertices ordered counterclockwise.

Contour matching. Suppose we have two groups of reconstructed 3D partial scans $\mathcal{P} = \{P_i\}_{i=0}^{n-1}$ and $\mathcal{Q} = \{Q_j\}_{j=0}^{n-1}$, respectively for the front sides and back sides of a group of n fragments scanned in a batch. We first extract their projected 2D contours, denoted as the groups $C_{\mathcal{P}}$ and $C_{\mathcal{Q}}$, and compute their shape descriptors of each contour in both groups. Recall that the contours in $C_{\mathcal{Q}}$ need to be flipped before computing their shape descriptors.

Next, for each scan P_i in the front batch \mathcal{P} , with its 2D projected contour denoted as C_{P_i} , we run through the set \mathcal{Q} of back side scans to find contour C_{Q_j} whose shape descriptor matches that of C_{P_i} the best, i.e. with the minimum matching error among all the scans in \mathcal{Q} . Specifically, we use L_2 norm to measure the difference $E(C_{P_i}, C_{Q_j})$ between the shape descriptors of two contours as two vectors. That is

$$E(C_{P_i}, C_{Q_j}) = \min_{0 \leq k \leq n_c-1} \|\Theta(P_i; v_0, \chi) - \Theta(Q_j; u_k)\|_2, \quad (1)$$

where v_0 is the first vertex of C_{P_i} , and u_k the k -th vertex of C_{Q_j} .

4.2 Registering the Front and Back Sides

After each fragment's front and back sides are paired, we then register them to get a complete 3D sherd model. Note that this is a very challenging problem because the two sides of a fragment usually share very small overlap, and the fracture regions often lack geometric features. In the previous Step 2, the shape descriptor matching produces a correspondence between the vertices of the two contours. This provides an initial alignment for registration. Specifically, from the vertex correspondence, we align the centroids of the two 3D contours and then use the algorithm of [Arun et al.

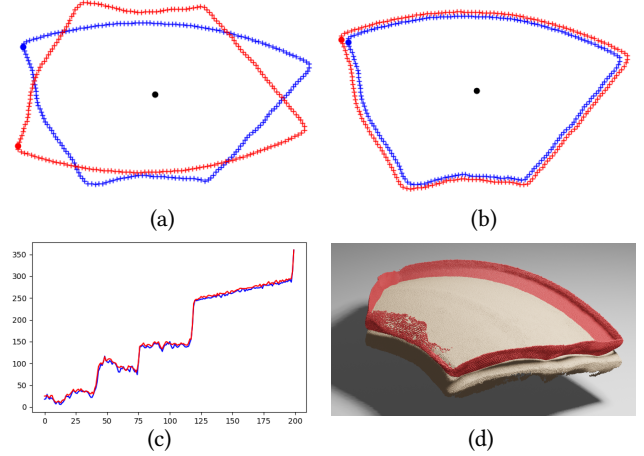


Fig. 4. **Contour matching.** (a) 2D contours for the front side (blue) and back side (red); (b) Matching of the two 2D contours; (c) The plots of the shape descriptors of the two matched contours; and (d) The initial alignment of the two corresponding 3D partial scans as suggested by the 2D contour matching. Here, for better visualization, only the rim region of the front scan on the top is shown (in red) in order to avoid occluding the back scan (shown in yellow) at the bottom.

1987] to find an optimal rigid transformation to align the partial 3D scans C_{P_i} and C_{Q_j} . This serves as a good initialization for the subsequent iterative registration.

Because of the small overlap between the two sides of the fragment, and the lack of salient textures and features in these regions, most existing registration methods tend to fail in their registrations. With common registration algorithms, it is hard to ensure that points (or a feature) from one side used in registration have proper corresponding points (or a feature) on the other side. Hence, we propose a *boundary-based ICP* method that utilizes 3D boundary points to iteratively search and minimize their distances to their corresponding points on the other side. Here the 3D boundary points refer to those points on the boundary of the front or back sides of the open point cloud surfaces. We use these 3D boundary points rather than all the points because the common overlap regions usually contain boundaries, hence, it is more likely for such boundary points to find their corresponding points (which may or may not be on boundary) from the other side.

3D boundary extraction. Each reconstructed front or back side of a sherd is a point cloud surface of open-disk topology, and therefore, has a boundary that contacts, or is near, the holding board of the turntable at the bottom. To extract the boundary points of a partial 3D scan, we followed the strategy in [Linsen 2001], but adopted the following procedure to improve efficiency. Given a reconstructed point cloud patch P , we identify boundary points by checking consistency from different views. First, a point p in P is projected to a pixel in input images where this point is visible. With the aid of masks generated for MVS reconstruction, we can determine whether a point in 3D is a candidate boundary point in one view. Specifically, we check the distance from p 's 2D projected point to the contour of the image mask. If this distance is smaller

than a threshold in all the images in which the point is visible, we take this point as a candidate boundary point. In this way, we obtain a candidate set of boundary points, and remove non-boundary points to improve efficiency. The candidate set may still contain some outliers (i.e., some non-boundary points that are very close to the boundary contour). We then apply the widely adopted boundary extraction method [Linsen 2001] to this candidate set to extract the final set of boundary points.

Bilateral Boundary ICP (BBICP). Next we use the extracted boundary points for model registration, i.e. computing a rigid transformation consisting of a rotation $R \in SO(3)$ and a translation $T \in \mathbb{R}^3$. Given two point clouds (front- and back-side partial models) \mathcal{P} and \mathcal{Q} as well as their boundary points $\mathcal{B}_\mathcal{P}$ and $\mathcal{B}_\mathcal{Q}$, the registration is performed by minimizing the sum of two terms: (1) one being the sum of the L_2 distances from the points in $\mathcal{B}_\mathcal{P}$ to their corresponding closest points in \mathcal{Q} , and (2) the other being the sum of the L_2 distances from the points in $\mathcal{B}_\mathcal{Q}$ to their corresponding closest points in \mathcal{P} .

We formulate this problem as an ICP optimization problem based on the correspondences of the boundary points and the point sets. Specifically, for each point $b_{P_i}^k \in B_{P_i}$, we find its closest point in Q_j , and denote the found correspondences as $K_1 = \{(b_{P_i}, q_j)\}$. Similarly, for each point $b_{Q_j}^l \in B_{Q_j}$, we find its closest point in P , and denote the correspondences as $K_2 = \{(p_i, b_{Q_j})\}$. We iteratively find the correspondences K_1 and K_2 and use the optimization method in [Ying et al. 2009] to compute the final transformation by iteratively minimizing

$$\epsilon^k(K_1, K_2) = \sum_{i=0}^{m-1} \|R^k b_{P_i}^k + T^k - q_i\|^2 + \sum_{j=0}^{n-1} \|R^k p_j + T^k - b_{Q_j}^l\|^2. \quad (2)$$

The ‘‘Boundary registration’’ sub-figure in the bottom right of Fig. 2 illustrates an example of this **bilateral boundary** registration. The two sides of a fragment are registered with the help of their boundary points (in red and blue, respectively). To better illustrate the idea of this BBICP algorithm, a 2D example is illustrated in Fig. 5. To register the red and the black shapes, we firstly find the correspondences between the black dots (boundary points of the black shape) and their nearest points in the red shape (the corners, marked with dashed black circles); then vice versa in the other direction. Through iteratively finding correspondence and solving relative transformation between the shapes, we optimize the registration between the red and black shapes. Finally, the red and black shapes are registered.

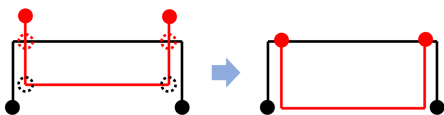


Fig. 5. 2D illustration of BBICP. The black points and red boundary points are matched with their corresponding points marked with dashed circles in the red scan and black scan, respectively.

5 EXPERIMENTS

We quantitatively evaluated our *FIRES* system. Since there is no public 3D fragment dataset available for systematic evaluation of such a capturing solution, we created a dataset and will release it to the public for comparisons (Sec. 5.1). With this dataset, *FIRES* is evaluated from two aspects: acquisition efficiency (Sec. 5.2) and reconstruction accuracy (Sec. 5.3). Our system was also tested and used at the excavation sites in Armenia. These field experiments, which further validated the efficacy of our system, will be reported in Sec. 5.4.

5.1 Dataset

We have built a sherd dataset to evaluate/compare sherd acquisition and 3D reconstruction. The dataset consists of the 3D scans of 123 fragments (some of which are shown in Fig. 6), with various shapes, sizes ($2\text{cm} \sim 15\text{cm}$ in diameter), and thicknesses ($0.3\text{cm} \sim 1\text{cm}$). These fragments were obtained by breaking several potteries, whose original geometry before breaking was also scanned. The 3D scan was done using a high-end EinScan Pro 2X [EinScan 2020] scanner in the fixed scan mode (under the highest precision), with a reported accuracy of 0.04mm . When scanning each fragment, we put it on the 3D scanner’s turntable to get 12 scans of its front side in a circle; then clipped the fragment to scan it vertically; and finally, scanned its back side. These partial scans were then merged to get a complete 3D model using software provided with the scanner. This dataset will be made public for comparative studies in fragment acquisition evaluation and related research such as 3D sherd reassembly and restoration.

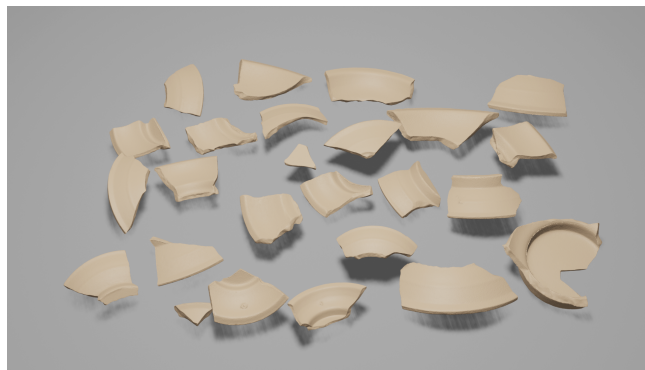


Fig. 6. A gallery of our reconstructed 3D sherds.

5.2 Acquisition Efficiency

Efficiency Estimation. We conducted lab experiments to scan all the 123 fragments in the dataset. The fragments were captured in 15 groups, with an average group size of 8.2 fragments. The turntable completes a full circle with 16 stops, in 1.7 minutes, capturing 48 images for the front sides of the fragments in one group. Then similarly, it uses 1.7 minutes to image the back sides of the same group. The manual operations to flip or replace a batch of sherds on the board took about 1.2 minutes to finish. Hence, given the average group size of 8.2 sherd pieces, scanning each piece’s both sides

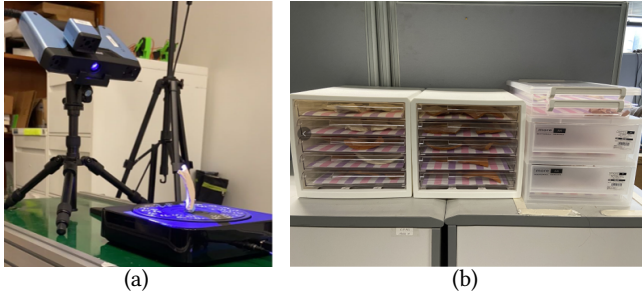


Fig. 7. 3D scanning and organization of fragments in our dataset. (a) shows the scanning process of fragments using EinScan, where a fragment is fixed upright on the turntable by a clip. (b) shows that all fragments are stored in a set of layered storage boxes.

took roughly $\frac{1.7 \times 2 + 1.2}{8.2} = 0.56$ minutes (34 seconds). This scales to scanning about 106 fragments in one hour, or about 800 fragments in one day of 8 working hours. The actual field test of the FIRES system at an excavation site in Armenia (Section 5.4) delivered an average throughput of capturing over 700 fragments in each 8-hour working day, during which short breaks were taken by the operator. Such capturing efficiency well meets the throughput requirement in archaeological fieldwork.

Table 1. Comparison of data acquisition efficiency per hour by different methods. Throughput: the number of fragments which can be scanned within one work hour. Fragment type: the type of fragments used by the corresponding method; Method: capturing techniques, including Structured Light scanner(SL), Laser scanner(L) and Photogrammetry(P).

	Throughput	Fragment type	Method
[Brown et al. 2008]	10	Fresco	SL
[Brown et al. 2012]	20	Fresco	SL
[Fan et al. 2016]	3	Fresco	SL
[Magnani 2014]	1	Lithic	L
[Magnani 2014]	6	Lithic	P
[Porter et al. 2015]	5	Lithic	P
[Karasik 2008]	13	Pottery	P
Our EinScan scanner	3	Pottery	SL
Ours	106	Pottery	P

Efficiency Comparison. We compared efficiency of our system with several recent systems reported in literature. Table 1 lists different methods’ estimated throughput within one hour. Among these methods, the design of [Porter et al. 2015] is most similar to ours: their rig consists of a camera and a turntable. But this system uses a rubber eraser to support the stand of objects on the turntable, and it also needs users manually adjusting camera positions and manually performing post-processing operations to remove the extraneous parts. Manual operations are also required in [Magnani 2014]. All these requirements hamper their acquisition efficiency. Note that for the methods designed for fresco fragment digitization [Brown et al. 2012, 2008; Fan et al. 2016], although they tend to fail in capturing some sherd fragments whose geometry is curved

(because they assume the bottom side of fresco fragments is almost planar), we still list them in this table for efficiency comparison. The pottery fragment capturing system [Karasik and Smilansky 2008] cannot produce complete sherd models automatically, because of the occlusion from the clip that holds the fragments. All these issues make these methods fail to meet the archaeological requirements of digitalization. Please refer to Section 4 of the supplementary for more details about how these hourly throughput numbers were estimated. Note that a few recent acquisition systems, designed to scan general objects, such as [Kaskman et al. 2019], were not included in this comparison. Because they usually don’t consider the contact areas between scanned objects and the holder of the objects, which means their methods also cannot get complete models.

5.3 Reconstruction Accuracy

To evaluate reconstruction accuracy, we adopted four widely used metrics: *Accuracy (Accu)*, *Completeness (Comp)*, *Mean Absolute Error (MAE)*, and *Error Standard Deviation (SD)*. We adopted their common definitions from the widely used Middlebury Benchmark [Seitz et al. 2006]. Definition details can be found in Section 3 of the supplementary file. Given the reconstructed point cloud R of a sherd, we align it with its corresponding scanned ground truth model G in our dataset, using FGR [Zhou et al. 2016] (for global alignment first) and ICP [Besl and McKay 1992] (for local refinement). The reconstruction accuracy is then measured by the difference between R and G . Note that the methods listed in Table 1 only had their data acquisition efficiency reported, without quantitative accuracy evaluation. Therefore, we could not perform a comparison, and only reported accuracy of our FIRES system.

Table 2 reports the reconstruction accuracy of all the sherds in our dataset, captured in 15 groups. Our method has an average reconstruction *accuracy* $T_a = 0.15mm$, *completeness* $p_c = 96.00\%$, and mean absolute error $MAE = 0.09mm$. Note that according to the survey provided by the Middlebury Benchmark, the state-of-the-art (SOTA) MVS algorithms reach pixel level accuracy, namely, 90% reconstructed points have accuracy *within about one pixel* [Furukawa and Ponce 2009]. Our reconstruction reaches a similar accuracy: the average size of fragments in our experiment is about 60mm wide, which occupies about 400 pixels in the capture images. This means a pixel in the images can represent about 0.15mm (i.e., $0.15mm/pixel = 60mm/400pixels$), which is the average accuracy reported in Table 2. Note that our reconstruction error includes those from both our MVS and registration steps; our registration does not introduce additional significant error.

BBICP vs other Registration Methods. A key component of our proposed pipeline is the BBICP registration algorithm, which enables an automatic and effective model reconstruction. We compared BBICP with the three most widely used registration methods: 1) FGR [Zhou et al. 2016], 2) Super 4PCS [Mellado et al. 2014], and 3) ICP [Besl and McKay 1992], by replacing BBICP with each of them and comparing the final reconstruction accuracy.

In our experiments, these 3 methods yield 5.11mm, 4.84mm, 4.71mm accuracy respectively, with only 11.37%, 10.03%, 18.69% completeness. They failed to build correct correspondences to align the two

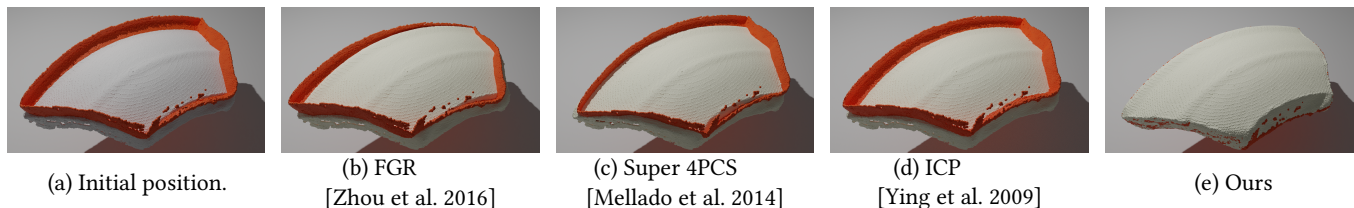


Fig. 8. Comparison of different registration algorithms. (a) The initial alignment of the front and back partial 3D scans. While our method is successful in this case, all the baseline methods fail to register the two scans, as there is obvious sliding error along the rim of the fragment.

Table 2. Quantitative accuracy evaluation of fragments reconstructed by FIREs. The 123 fragments in our dataset are evaluated, in 15 groups. ID: Group ID; Num: the *number* of fragments in a group; Acc.(mm): average Accuracy of reconstructed fragments in a group (smaller is better); Comp.(%): average Completeness of reconstructed fragments in a group (higher is better); MAE(mm): average Mean Absolute Error of reconstructed fragments in a batch; SD(mm): average Standard Deviation of reconstructed fragments in a group.

ID	Num	Accu.↓	Comp.↑	MAE↓	SD↓
1	9	0.14	98.5	0.08	0.06
2	9	0.14	98.39	0.08	0.06
3	7	0.15	93.74	0.09	0.06
4	9	0.15	97.27	0.08	0.07
5	8	0.11	98.47	0.07	0.06
6	8	0.12	97.64	0.07	0.05
7	8	0.13	96.80	0.07	0.07
8	9	0.19	95.65	0.10	0.07
9	9	0.19	94.42	0.10	0.08
10	7	0.13	98.53	0.08	0.06
11	7	0.16	90.88	0.09	0.07
12	4	0.20	90.75	0.10	0.10
13	4	0.16	95.92	0.09	0.11
14	7	0.15	98.12	0.09	0.09
15	18	0.15	94.95	0.08	0.06
Mean	8.2	0.15	96.00	0.09	0.07

sides of fragments. In contrast, our method can build high-quality models with **0.15mm accuracy and 96.00% completeness**.

In these experiments, through the initial front-back matching (Step 2), good initial global alignments between the front and back sides were obtained. However, these three baseline methods (FGR, Super 4PCS, and ICP) still often failed to correctly register the two sides. This is because the overlapping regions of the two scans are small and these fracture regions contain very few distinct features. Therefore, it is hard for these baseline methods to build reliable correspondences. In contrast, our BBICP can handle such cases more robustly. By building boundary-based correspondences, our method was able to identify more overlap regions stably and yield more accurate registration. Fig. 8 shows a registration example by different methods.

Archaeological Needs. In archaeology communities, the implications of automatic 3D scanning of fragments has not been well

explored. The field is still developing requirements/standards on how accurately pieces should be scanned. Given that almost all prior work for documenting and measuring sherds has been undertaken manually, any insertion of digital methods automatically increases accuracy significantly above the state-of-art in the field. The 3D models we created are more than sufficient for extracting 2D drawings for archaeological publications. Looking forward, our goal is to be as accurate as possible for the purposes of long-term archiving. We also plan to experiment with new analytical methods that are made possible by this new large-scale dataset, such as reassembling whole vessels back together. These future efforts will, in turn, inform the field of archaeology about whether our current accuracy is already sufficient for these more detailed analyses or if we need to continue to improve accuracy.

5.4 Field Experiments

This FIREs system was deployed for use at the excavation site of the Ararat Plain Southeast Archaeological Project (APSAP) in Armenia in the summer of 2022 for two and half months. During this period, over 20,000 ceramic fragments were excavated, requiring rapid digital recording for downstream analysis and other applications. Fig. 9 shows the excavation site (a), some excavated fragments (b), our device deployed in a local private residence (c) which was adapted for use as a field lab, and some reconstructed models (d).

Archaeologists were able to deploy our device easily on the site, and used it to achieve a throughput of about 730 fragments per day. In a real-world situation, the field lab is a busy and complicated environment that includes the comprehensive data collection process before and after 3D scanning. In our case, the number of sherds scanned day-to-day varied based on many factors. The operator of the 3D scanner has multiple tasks, from changing camera batteries and making sure the cameras remained aligned, to managing the locations of the bags of sherds. The operator had to track bags that were coming in for scanning, those that were finished scanning, and had to organize the storage of completed bags into plastic boxes. The human operator also cannot work continuously, and needs to take periodic breaks. Therefore, the capturing throughput in the field (i.e., 730 fragments per day of 8 working hours) is slightly lower than the estimation from the lab testing (i.e., 800 pieces per day, extrapolated from about 100 fragments in one hour).

We also quantitatively evaluated the reconstructed models from the site to test the field acquisition accuracy. Archaeologists randomly selected 26 fragments among more than 200 groups and



Fig. 9. **System deployment in Armenia.** (a) The excavation site; (b) The excavated fragments; (c) Our device deployed on the site; (d) Reconstructed 3D fragments.

scanned their corresponding ground-truth 3D models through EinScan [EinScan 2020]. We then compared their 3D models reconstructed using our FIRES system with their corresponding GT 3D models. The average reconstruction accuracy of these 26 fragments is about 0.16mm, which is similar to our lab experiments (0.15mm accuracy, see Table 2). This validates our system’s robustness in capturing accuracy when deployed in the field. The efficiency of initial data capture has opened new challenges downstream with data upload and then the building of 3D models, which currently takes manual oversight and significant server time.

The successful large-scale capturing experiment at the excavation site confirmed the feasibility and practicability of our *FIRES* system. Before our system, previous attempts all failed to provide such a *practical solution to fast, accurate, and reliable digitization of a large number of sherds*, which has been a long-standing problem in archaeology excavation. We will make our system and dataset publicly available and believe it can significantly alleviate the burden of archaeologists and boost the downstream applications, such as relic re-assembly.

5.5 Limitations

Capturing Textureless Sherds. The image based reconstruction relies on textural features to reconstruct surfaces, and its performance may drop when processing textureless fragments. The final reconstruction accuracy of such fragments can be lower. One possible solution can be applying some scanning sprays (e.g. talc developer spray [Porter et al. 2015]) to improve the reconstruction quality, though this intervention might not be suitable for ancient objects and would take manual time.

Failure cases. If some fragments in a batch have very similar 2D contours or some fragments themselves are symmetrical (e.g., fragments with circular shapes), then our contour-based matching method may fail due to ambiguities. In this case, one may use fragment locations (as discussed in Section 4.1) to help resolve the matching ambiguity. It may also be possible to manipulate the manual sorting and placement process slightly to counter these effects.

6 CONCLUSIONS AND FUTURE WORK

We proposed the *FIRES* system, which consists of an image capturing device and a 3D reconstruction pipeline, for efficient image

acquisition and reconstruction of archaeological sherds. Our system had been deployed and used at an excavation site in summer 2022. The field tests confirmed that *FIRES* is easy to deploy and can capture more than 700 ceramic fragments in eight hours and ultimately generate high-quality reconstructed models with about 0.16mm accuracy. This system provides the first promising solution to meet the practical demand of archaeological field work. And we will continue to work on improving the downstream 3D processing efficiency.

ACKNOWLEDGMENTS

We would like to thank all the people who have provided helpful suggestions and feedback for this project, especially Lei Yang and Cheng Lin.

REFERENCES

- Namir Ahmed, Michael Carter, and Neal Ferris. 2014. Sustainable archaeology through progressive assembly 3D digitization. *World Archaeology* 46, 1 (2014), 137–154.
- Dror Aiger, Niloy J Mitra, and Daniel Cohen-Or. 2008. 4-points congruent sets for robust pairwise surface registration. In *ACM SIGGRAPH 2008 papers*. 1–10.
- K Somani Arun, Thomas S Huang, and Steven D Blostein. 1987. Least-squares fitting of two 3-D point sets. *IEEE Transactions on pattern analysis and machine intelligence* 5 (1987), 698–700.
- Yusuf Abdullahi Badamasi. 2014. The working principle of an Arduino. In *2014 11th international conference on electronics, computer and computation (ICECCO)*. IEEE, 1–4.
- Fausto Bernardini and Chandrajit L Bajaj. 1997. Sampling and reconstructing manifolds using alpha-shapes. (1997).
- Paul J Besl and Neil D McKay. 1992. A method for registration of 3-D shapes. In *Sensor fusion IV: control paradigms and data structures*, Vol. 1611. Spie, 586–606.
- Benedict Brown, Lara Laken, Philip Dutré, Luc Van Gool, Szymon Rusinkiewicz, and Tim Weyrich. 2012. Tools for virtual reassembly of fresco fragments. *International journal of heritage in the digital era* 1, 2 (2012), 313–329.
- Benedict J Brown, Corey Toler-Franklin, Diego Nehab, Michael Burns, David Dobkin, Andreas Vlachopoulos, Christos Doumas, Szymon Rusinkiewicz, and Tim Weyrich. 2008. A system for high-volume acquisition and matching of fresco fragments: Reassembling Thera wall paintings. *ACM transactions on graphics (TOG)* 27, 3 (2008), 1–9.
- Dan Cernea. 2020. OpenMVS: Multi-View Stereo Reconstruction Library. (2020). <https://cdseacave.github.io/openMVS>
- Dmitry Chetverikov, Dmitry Svirko, Dmitry Stepanov, and Pavel Krsek. 2002. The trimmed iterative closest point algorithm. In *Object recognition supported by user interaction for service robots*, Vol. 3. IEEE, 545–548.
- Peter J. Cobb, John H. Sigmier, Petra M. Creamer, and Emily R. French. 2019. Collaborative Approaches to Archaeology Programming and the Increase of Digital Literacy Among Archaeology Students. *Open Archaeology* 5, 1 (2019), 137–154.
- L Di Angelo, P Di Stefano, and C Pane. 2018. An automatic method for pottery fragments analysis. *Measurement* 128 (2018), 138–148.
- EinScan 2020. EinScan Pro 2X. <https://www.einscan.com/handheld-3d-scanner/einscan-pro-2x/>.

- Xinyi Fan, Linguang Zhang, Benedict Brown, and Szymon Rusinkiewicz. 2016. Automated view and path planning for scalable multi-object 3D scanning. *ACM Transactions on Graphics (TOG)* 35, 6 (2016), 1–13.
- Yasutaka Furukawa and Jean Ponce. 2009. Accurate, dense, and robust multiview stereopsis. *IEEE transactions on pattern analysis and machine intelligence* 32, 8 (2009), 1362–1376.
- Sergio Garrido-Jurado, Rafael Muñoz-Salinas, Francisco José Madrid-Cuevas, and Manuel Jesús Marín-Jiménez. 2014. Automatic generation and detection of highly reliable fiducial markers under occlusion. *Pattern Recognition* 47, 6 (2014), 2280–2292.
- T. Hodan, P. Haluza, Š. Obržálek, J. Matas, M. Lourakis, and X. Zabulis. 2017. T-LESS: An RGB-D Dataset for 6D Pose Estimation of Texture-Less Objects. In *2017 IEEE Winter Conference on Applications of Computer Vision (WACV)*. 880–888. <https://doi.org/10.1109/WACV.2017.103>
- Avshalom Karasik and Uzy Smilansky. 2008. 3D scanning technology as a standard archaeological tool for pottery analysis: practice and theory. *Journal of Archaeological Science* 35, 5 (2008), 1148–1168.
- R. Kaskman, S. Zakharov, I. Shugurov, and S. Ilic. 2019. HomebrewedDB: RGB-D Dataset for 6D Pose Estimation of 3D Objects. In *2019 IEEE/CVF International Conference on Computer Vision Workshop (ICCVW)*. 2767–2776. <https://doi.org/10.1109/ICCVW.2019.00338>
- Alexander Kasper, Zhixing Xue, and Rüdiger Dillmann. 2012. The KIT object models database: An object model database for object recognition, localization and manipulation in service robotics. *The International Journal of Robotics Research* 31, 8 (2012), 927–934. <https://doi.org/10.1177/0278364912445831> arXiv:<https://doi.org/10.1177/0278364912445831>
- Morag M. Kersel. 2015. Storage Wars: Solving the Archaeological Curation Crisis? *Journal of Eastern Mediterranean Archaeology and Heritage Studies* 3, 1 (2015), 42–54.
- Lars Linsen. 2001. *Point cloud representation*. Univ., Fak. für Informatik, Bibliothek Technical Report, Faculty of Computer ...
- Matthew Magnani. 2014. Three-dimensional alternatives to lithic illustration. *Advances in Archaeological Practice* 2, 4 (2014), 285–297.
- Nicolas Mellado, Dror Aiger, and Niloy J Mitra. 2014. Super 4pcs fast global pointcloud registration via smart indexing. In *Computer Graphics Forum*, Vol. 33. Wiley Online Library, 205–215.
- François Pomerleau, Francis Colas, Roland Siegwart, and Stéphane Magnenat. 2013. Comparing ICP variants on real-world data sets. *Autonomous Robots* 34, 3 (2013), 133–148.
- Samantha T Porter, Morgan Roussel, and Marie Soressi. 2015. A simple photogrammetry rig for the reliable creation of 3D artifact models in the field: lithic examples from the Early Upper Paleolithic sequence of Les Cottés (France). (2015).
- Olaf Ronneberger, Philipp Fischer, and Thomas Brox. 2015. U-net: Convolutional Networks for Biomedical Image Segmentation. In *International Conference on Medical image computing and computer-assisted intervention*. Springer, 234–241.
- Christopher H. Roosevelt, Peter J. Cobb, Emanuel Moss, Brandon Olson, and Sinan Ünüsoy. 2015. Excavation is Destruction Digitization: Advances in Archaeological Practice. *Journal of Field Archaeology* 40, 3 (2015), 325–346.
- Radu Bogdan Rusu, Nico Blodow, and Michael Beetz. 2009. Fast point feature histograms (FPFH) for 3D registration. In *2009 IEEE international conference on robotics and automation*. IEEE, 3212–3217.
- Philip Sapirostein. 2018. A high-precision photogrammetric recording system for small artifacts. *Journal of Cultural Heritage* 31 (2018), 33–45.
- Thomas W Sederberg, Peisheng Gao, Guojin Wang, and Hong Mu. 1993. 2-D shape blending: an intrinsic solution to the vertex path problem. In *Proceedings of the 20th annual conference on Computer graphics and interactive techniques*. 15–18.
- Steven M Seitz, Brian Curless, James Diebel, Daniel Scharstein, and Richard Szeliski. 2006. A comparison and evaluation of multi-view stereo reconstruction algorithms. In *2006 IEEE computer society conference on computer vision and pattern recognition (CVPR'06)*, Vol. 1. IEEE, 519–528.
- A. Singh, J. Sha, K. S. Narayan, T. Achim, and P. Abbeel. 2014. BigBIRD: A large-scale 3D database of object instances. In *2014 IEEE International Conference on Robotics and Automation (ICRA)*. 509–516. <https://doi.org/10.1109/ICRA.2014.6906903>
- Gary KL Tam, Zhi-Quan Cheng, Yu-Kun Lai, Frank C Langbein, Yonghuai Liu, David Marshall, Ralph R Martin, Xian-Fang Sun, and Paul L Rosin. 2012. Registration of 3D point clouds and meshes: A survey from rigid to nonrigid. *IEEE transactions on visualization and computer graphics* 19, 7 (2012), 1199–1217.
- Svante Wold, Kim Esbensen, and Paul Geladi. 1987. Principal component analysis. *Chemometrics and intelligent laboratory systems* 2, 1-3 (1987), 37–52.
- Jiaolong Yang, Hongdong Li, Dylan Campbell, and Yunde Jia. 2015. Go-ICP: A globally optimal solution to 3D ICP point-set registration. *IEEE transactions on pattern analysis and machine intelligence* 38, 11 (2015), 2241–2254.
- Shihui Ying, Jigen Peng, Shaoyi Du, and Hong Qiao. 2009. A scale stretch method based on ICP for 3D data registration. *IEEE Transactions on Automation Science and Engineering* 6, 3 (2009), 559–565.
- Qian-Yi Zhou, Jaesik Park, and Vladlen Koltun. 2016. Fast global registration. In *European Conference on Computer Vision*. Springer, 766–782.